Atmospheric Research 193 (2017) 36–49

Contents lists available at ScienceDirect

Atmospheric Research

journal homepage: www.elsevier.com/locate/atmosres

Intercomparison of PERSIANN-CDR and TRMM-3B42V7 precipitation estimates at monthly and daily time scales

Pari-Sima Katiraie-Boroujerdy[a,*], Ata Akbari Asanjan[b], Kuo-lin Hsu[b], Soroosh Sorooshian[b]

[a] Department of Meteorology, Faculty of Marine Science and Technology, Tehran North Branch, Islamic Azad University, Tehran, Iran
[b] Center for Hydrometeorology and Remote Sensing (CHRS), The Henry Samueli School of Engineering, Department of Civil and Environmental Engineering, University of California, Irvine, CA 92697, USA

ARTICLE INFO

Keywords:
Three cornered hat
Satellite data
Precipitation
Remote sensing
Iran
Evaluation
Extremes

ABSTRACT

In the first part of this paper, monthly precipitation data from Precipitation Estimation from Remotely Sensed Information using Artificial Neural Networks–Climate Data Record (PERSIANN-CDR) and Tropical Rainfall Measuring Mission 3B42 algorithm Version 7 (TRMM-3B42V7) are evaluated over Iran using the Generalized Three-Cornered Hat (GTCH) method which is self-sufficient of reference data as input. Climate Data Unit (CRU) is added to the GTCH evaluations as an independent gauge-based dataset thus, the minimum requirement of three datasets for the model is satisfied. To ensure consistency of all datasets, the two satellite products were aggregated to 0.5° spatial resolution, which is the minimum resolution of CRU. The results show that the PERSIANN-CDR has higher Signal to Noise Ratio (SNR) than TRMM-3B42V7 for the monthly rainfall estimation, especially in the northern half of the country. All datasets showed low SNR in the mountainous area of southwestern Iran, as well as the arid parts in the southeast region of the country. Additionally, in order to evaluate the efficacy of PERSIANN-CDR and TRMM-3B42V7 in capturing extreme daily-precipitation amounts, an in-situ rain-gauge dataset collected by the Islamic Republic of the Iran Meteorological Organization (IRIMO) was employed. Given the sparsity of the rain gauges, only 0.25° pixels containing three or more gauges were used for this evaluation. There were 228 such pixels where daily and extreme rainfall from PERSIANN-CDR and TRMM-3B42V7 could be compared. However, TRMM-3B42V7 overestimates most of the intensity indices (correlation coefficients; R between 0.7648–0.8311, Root Mean Square Error; RMSE between 3.29mm/day-21.2mm/5day); PERSIANN-CDR underestimates these extremes (R between 0.6349–0.7791 and RMSE between 3.59mm/day-30.56mm/5day). Both satellite products show higher correlation coefficients and lower RMSEs for the annual mean of consecutive dry spells than wet spells. The results show that TRMM-3B42V7 can capture the annual mean of the absolute indices (the number of wet days in which daily precipitation > 10 mm, 20 mm) better than PERSIANN-CDR. The results of daily evaluations show that the similarity of Empirical Cumulative Density Function (ECDF) of satellite products and IRIMO gauges daily precipitation, as well as dry spells with different thresholds in some selected pixels (include at least five gauges), are significant. The results also indicate that ECDFs become more significant when threshold increases. In terms of regional analyses, the higher SNR of the products on monthly (based on the GTCH method) and daily evaluations (significant ECDFs) is mostly consistent.

1. Introduction

Accurate estimation of precipitation is critical for a comprehensive understanding of hydrological and climate analyses, especially for arid countries such as Iran. The ground (in-situ) and remote-sensing (satellite and radar) observations are frequently used for precipitation estimation (Tapiador et al., 2012). Rain gauges provide a direct measurement of precipitation, despite the fact that their measurements are at point scale, and the distribution of gauges is very sparse, especially in mountainous and desert areas. Apart from sampling error (for rain-gauge measurements), extending precipitation data from the point scale to the spatial scale is another source of bias (Wood et al., 2000; Villarini et al., 2008). The various statistical and interpolation methods which have been applied to derive gridded ground-based precipitation data are also one of the main contributors to error (New et al. 1999; Tapiador et al. 2012).

Satellite-based precipitation products are available globally and can effectively extend precipitation measurements to regions where con-

* Corresponding author.
E-mail addresses: sima_katiraie@yahoo.com, pkatirai@uci.edu (P.-S. Katiraie-Boroujerdy).

http://dx.doi.org/10.1016/j.atmosres.2017.04.005
Received 12 August 2016; Received in revised form 22 March 2017; Accepted 3 April 2017
Available online 04 April 2017
0169-8095/

ventional in-situ data are not available. However, the satellite-based precipitation products are subject to various sources of bias, including sampling, sensing, and estimation-algorithm bias. To respond to the great potential for the wide range of applications of satellite-based precipitation products, many evaluation studies have been conducted to understand and determine their error characteristics (e.g., Arkin and Xie, 1994; Adler et al., 2001; Hossain and Huffman, 2008; Tian et al., 2009; Shen et al., 2010; Kidd et al., 2012; Tong et al., 2014; Conti et al., 2014; Prakash et al., 2015; Zhu et al., 2016; Liu et al., 2016). The studies have shown that the evaluation results of precipitation products can be sensitive to the selected regions of varying climate, geography, and topography. Among those evaluations, only limited studies have been conducted over Iran. For example, Javanmard et al. (2010) evaluated the TRMM-3B42V6 precipitation data with a 0.25° × 0.25° latitude-longitude gridded rain-gauge data over Iran for the period 1998–2006. Their results show that TRMM-3B42V6 underestimates the annual average precipitation for each grid cell over the entire country, specifically the Caspian Sea, and the Zagros Mountainous region by 0.17, 0.39, and 0.15 mm/day, respectively. The results from the comparisons of four satellite based precipitation datasets including CPC Morphing Technique; CMORPH, PERSIANN, adjusted PERSIANN and TRMM-3B42V6, with rain gauge data over Iran were recently presented by Katiraie-Boroujerdy et al., (2013). They show that: 1) although all satellite products detect spring precipitation more than winter precipitation, especially for the mountainous areas, they underestimate annual precipitation over the Caspian Sea coastal regions and 2) the adjusted PERSIANN and TRMM-3B42V6 provide better estimates than CMORPH over Zagros Mountainous regions. Moazami et al. (2013) verified PERSIANN, TRMM-3B42V7 and TRMM-3B42RT daily rain rates using rain gauge observations over Iran for 47 rainfall events during 2003–2006. The spatially averaged results over the country show that TRMM-3B42V7 estimates daily rain rates better than PERSIANN and TRMM-3B42RT. This result is to be expected since TRMM-3B42V7 is a gauge-adjusted product. In the same study the authors show that while PERSIANN has greater probability of detection of rainfall events, its false alarm ratio is worse than the other products. Although rain-gauge data are used as reference (or “truth”) in most satellite-evaluation studies, as mentioned above, the rain-gauge datasets are still subject to different kinds of errors (Habib et al., 2001; Habib and Krajewski, 2002; Krajewski et al., 2006; Ciach and Krajewski, 2006). Furthermore, in some areas such as Iran, a reliable, continuous (spatial and temporal) gridded-precipitation dataset is not available. Therefore, instead of using an ideal precipitation dataset as reference data, a new method is required that can be used for evaluation of precipitation estimations without depending on a certain reference dataset (“truth”).

In this paper, the GTCH (Galindo and Palacio, 1999) is employed to assess the relative performances of two satellite-based precipitation datasets at the monthly scale. Although the GTCH method has been used for atmospheric-angular momentum and clock-instability estimation (Koot et al., 2006; Premoli and Tavella, 1993), the application of this method for an evaluation of a precipitation dataset remains very limited (Awange et al., 2015). Unlike the traditional method for evaluation, this method does not need reference data and is suitable for desert and mountainous areas, such as Iran, where reliable continuous spatial and temporal in-situ data are not always available. Although a reference dataset is not required, at least 3 datasets are required for calculations. It is worth mentioning that similar procedure has recently been used for assessment of remote sensing soil moisture datasets (Gruber et al. 2016). The two main differences between the Triple Collocation (TC) method used by Gruber et al., 2016 and our approach are 1) the assumption of uncorrelation between errors and datasets which might not be the case for this study and 2) GTCH allows choosing more than three datasets which is not possible in TC method.

The two satellite-based precipitation observation products used in this study were the PERSIANN-CDR and TRMM-3B42V7. The third dataset chosen is the gauge-based precipitation dataset known as CRU. The period selected for the monthly evaluation was 1998–2007, which overlaps with the period for which IRIMO data are available. The reason for this comparison is to assess the relative accuracy of the recently released PERSIANN-CDR, which is a 33 + years, high-resolution (daily, 0.25°) satellite product suitable for the study of hydrologic extremes. The choice of the TRMM-3B42V7 and CRU datasets was because the former is often used as a benchmark for satellite-product comparisons, and the latter is a gauge-based gridded dataset. The spatial resolution for the monthly evaluation was 0.5°, which is the resolution of CRU data. Additionally, for evaluating the efficacy of the PERSIANN-CDR in capturing extreme daily-precipitation amounts, an in-situ rain-gauge dataset collected by the IRIMO was employed (hereafter: GAUGE data). For this component of the evaluation, only 0.25° pixels containing 3 or more gauges were used. There were 228 such pixels where daily and extreme rainfall data from PERSIANN-CDR and TRMM-3B42V7 could be compared. All of the assessments were performed over the period of 1998–2007. The reason for the selection of this time period was because the daily rain-gauge data (GAUGE) were only available for this period.

The GTCH method can assess each dataset by taking the error subtraction of each pair of datasets and using the back propagation of error to search for the uncertainty within each product. This method assumes that the errors within the data are normally distributed and, by finding the “imprecision of measurement”, we can determine the bias (Grubbs, 1948). Thus, we can estimate the uncertainty of each dataset using the proposed method without taking any reference among them. The problem is defined in a way to reach the global minimum in the defined boundary and, therefore, it will have a unique solution. This ability of the GTCH can help us obtain most accurate comparison in term of uncertainty.

In this paper, in addition to extreme evaluation, we compared the ECDFs of daily precipitation as well as dry spells with different thresholds (2.5, 5, and 10 mm/day) in seven selected 0.25° pixels that include at least five gauges for PERSIANN-CDR, TRMM-3B42V7, and GAUGE. We chose these pixels based on the regional performance of the satellite products at monthly scales. In this paper, the performance is defined and compared based on Signal to Noise ratio, RMSE and correlation coefficient.

This paper is organized as follow. The study area and data that are used in this study are presented in Section 2. The GTCH method is described in Section 3. Data assessment is presented in Section 4. Finally, the conclusions are summarized in Section 5.

2. Study area and datasets

The study area covers Iran, located in a dry subtropical area, extending from 25°N-40°N latitude and from 44°E-64°E longitude, with the Caspian Sea to the north and the Persian Gulf and Sea of Oman to the south (Fig. 1). Iran is located in a semi-arid-to-arid region, with dry, hot deserts in the central, eastern, and southeastern areas of the country. Two high mountain ranges, the Alborz Mountains in the north and the Zagros Mountains in the west, have a significant impact on the precipitation patterns. Most of the rainfall is produced by the Mediterranean and Sudan Lows, occurring in the winter and early spring months. While mean annual precipitation is less than 250 mm, it falls unevenly, with less than 50 mm in the desert areas and more than 1000 mm along the coastline of the Caspian Sea to the north.

2.1. Datasets

Four precipitation datasets with different spatial and temporal resolutions are used in this study for the period of 1998–2007 (the available rain-gauge time period). PERSIANN-CDR and TRMM-3B42V7 data are satellite-based, and CRU and GAUGE in-situ data are gauge-based. However, the daily precipitation of global datasets is from 00

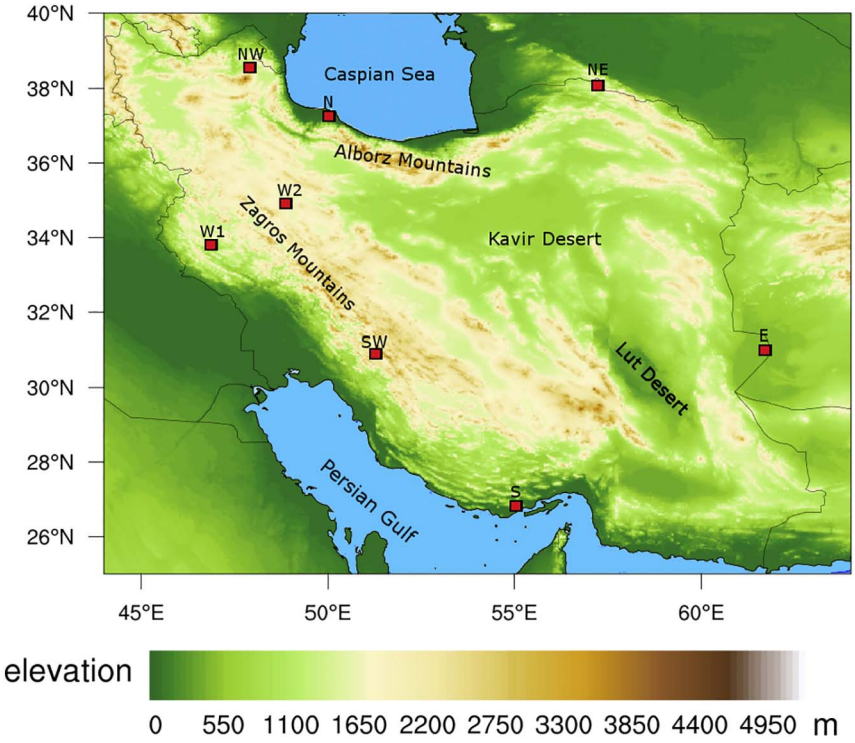

Fig. 1. The topography and location of Iran and eight selected pixels for daily analyses.

UTC-24 UTC; the rain-gauge precipitation data are measured in local time so that the precipitation is accumulated from 15 UTC for 24 h and reported as daily precipitation all over Iran. Therefore, the 3-hourly PERSIANN-CDR and TRMM-3B42V7 data are used to produce the daily-precipitation data consistent with the temporal scale of the rain-gauge data (i.e., 15–15 UTC) during the study time period (1998–2007). As a 0.1 mm/h threshold is considered to produce the 3-hourly PERSIANN-CDR data, in order to reduce the uncertainties in the analysis and also as we are going to focus on extremes, a 2.5 mm/day threshold is considered for daily-precipitation calculations for all datasets, and every daily-precipitation amount less than 2.5 mm/day is considered as zero.

2.1.1. Gauge Measurements

More than 2100 rain-gauge daily time series in Iran for the period of 1998–2007 were used in this study. The GAUGE data were provided by IRIMO. Both gauge and satellite datasets were processed to the spatial resolution of 0.25° × 0.25° latitude-longitude grids for product evaluation (Katiraie-Boroujerdy et al., 2013). To reduce the uncertainty of point measurements from gauges, only grid boxes that contained at least 3 gauges were included in the evaluation (Adler et al., 2003; Yong et al., 2013; Xue et al., 2013). Under these criteria, 228 pixels were selected. These pixels are distributed all over Iran, mostly condensed in some mountainous areas but sparse in the deserts regions (Fig. 7).

2.1.2. PERSIANN-CDR

PERSIANN-CDR is a daily global-precipitation dataset which extends from 60°S- 60°N and is available from 1983-present (Ashouri et al., 2015). This product applies the basic PERSIANN algorithm (Sorooshian et al., 2000) to estimate precipitation from satellite imagery every 3 h. These 0.25° 3-hourly rainfall rate estimates are accumulated to the monthly precipitation at 2.5°. Spatial and temporal patterns of PERSIANN estimation are adjusted further based on monthly rainfall estimated from Global Precipitation Climate Project (GPCP; Huffman et al. 2001), for more information see http://www1.ncdc.noaa.gov/pub/data/sds/cdr/CDRs/PERSIANN/ Algorithm Description.pdf. For better fitting to the daily-accumulation rainfall from gauges, daily rainfall from PERSIANN-CDR data is processed based on 3-hourly precipitation estimation.

2.1.3. TRMM-3B42V7

The TRMM-3B42V7 data are generated by merging satellite and ground observations (see ftp://meso-a.gsfc.nasa.gov/pub/trmmdocs/3B42_3B43_doc.pdf and Huffman et al., 2007). This dataset is available from 50°S–50°N, starting from 1998 present (there is a delay of about 2 months). The data are processed using available passive microwave precipitation samples from 3-hour averages. The coverage gaps are filled with calibrated IR data. Finally, the monthly rain-gauge and monthly accumulated multi-satellite data are combined to produce 3B43 data. Then, these data are used to derive 3-hourly TRMM data to produce TRMM-3B42V7 data. In this study, we used TRMM-3B42V7 0.25°data accumulated daily from 3-hourly precipitation consistent with rain-gauge local-time accumulation data.

2.1.4. CRU

The CRU data are constructed from monthly observations using about 4000 meteorological stations across the world (excluding Antarctica and only over land areas). Obviously these data are available only on monthly temporal resolution. These datasets are gridded to 0.5° resolution and include monthly time series of precipitation, daily maximum and minimum temperatures, and other variables for 1901–2013 (CRU TS3.22 is a recent release; Harris et al., 2014).

For spatial consistency in monthly evaluation, the PERSIANN-CDR and TRMM-3B42V7 data are aggregated to 0.5° using bilinear interpolation, for which the CRU dataset is available. Bilinear interpolation will take the average of neighboring pixels in both latitude and longitude axes. On the other hand, the daily comparisons are conducted in 0.25° spatial resolution for which all datasets (PERSIANN-CDR, TRMM-3B42V7, and GAUGE) are available. For the few days and few pixels where there are some missing data in both satellite and gauge data, the daily evaluations are employed for days that both satellite and GAUGE data are available. As mentioned previously, for temporal consistency between monthly and daily evaluations, the time period of 1998–2007, for which the GAUGE dataset is available is used.

3. Methods

The major challenge with evaluating a precipitation dataset (mainly satellite-based) is the lack of condense, continuous, and well-distributed rain-gauge network data. Conventional rain-gauge observations are usually considered as accurate precipitation; however, in some areas, such as Iran, a reliable full-spatial coverage rain-gauge dataset does not exist. Therefore, in the first part of this study, the assessment is limited to monthly intercomparisons of different datasets without any reference (or preferred) dataset. Mean Difference (MD) and Root Mean Square Difference (RMSD) between monthly data at each pixel are calculated using the following formulas:

$$MD = \frac{\sum_{i=1}^{N} [P1(i) - P2(i)]}{N} \tag{1}$$

$$RMSD = \sqrt{\frac{\sum_{i=1}^{N} [P1(i) - P2(i)]^2}{N}} \tag{2}$$

where $P1$, $P2$ are the monthly precipitation (in millimeters) for datasets 1 and 2, and N shows the total number of months (here, 120) in each pixel. However, MD represents how two estimates match in average; RMSD measures the sample standard difference between two products. In fact, MD shows underestimation or overestimation of the two data in average in different parts of the study area. RMSD accumulates the magnitudes of the differences between two products for various times into a single measure of difference quantity.

The spatial correlation coefficient is used to show a linear relationship between the spatial distribution of the satellite products and GAUGE annual mean of the extreme indices in the study area. The most commonly used Pearson correlation coefficient (R) between satellite estimate P_{Si} and gauge observation P_{Gi} at each pixel (i) is defined as:

$$R = \frac{\sum_{i=1}^{N} (P_{Si} - \overline{P_S})(P_{Gi} - \overline{P_G})}{\sqrt{\sum_{i=1}^{N} (P_{Si} - \overline{P_S})^2 \sum_{i=1}^{N} (P_{Gi} - \overline{P_G})^2}} \tag{3}$$

where N is the number of the selected pixels in the study area and $\overline{P_S}$ and $\overline{P_G}$ are the average of P_{Si} and P_{Gi} for all the selected pixels. The closer R to $+1$ shows the stronger agreement between the spatial distribution of the satellite estimations and the gauge observations. Because the CRU monthly data are available only in 0.5° spatial resolution for consistency, the PERSIANN-CDR and TRMM-3B42V7 data are regridded to 0.5° resolution.

3.1. The generalized three-cornered hat method

The Three-Cornered Hat (TCH) method is derived from the Gauss-Markov theorem on the basic premise (Galindo and Palacio, 1999) that the Ordinary Least Square estimator can be used as the best linear unbiased estimator in the case of the equal variance and error expectations equal to zero for the uncorrelated datasets (Larocca, 2010). Tavella and Premoli (1994) reconsidered the assumption of uncorrelation and derived a GTCH method applicable for both uncorrelated and correlated datasets.

For the precipitation dataset, all data of the time-series will have a portion of true data, which are called signal, and a noisy portion accompanying the signal. Hence, the data for each time step could be noted as:

$$x_{i,j} = S_{i,j} + n_{i,j} \quad ji \in \{1,\forall N\}, \quad j \in \{1,\ldots,M\} \tag{4}$$

where N is the number of rainfall products that are intended to be compared and M is the number of months recorded in data. Additionally, S represents the signal and n would be the Gaussian noise.

Let $\{x_i\}_{i=1\ldots N}$ and $\{n_i\}_{i=1\ldots N}$ represent the time series of N products and their noises, respectively. Then, by taking deference between the products, we will obtain:

$$y_i = x_i - x_R = n_i - n_R \qquad \forall\, i \in \{1,\ N-1\}$$

$$Y_{M\times N-1} = [y_1 \quad y_2 \cdot \ \cdot \ y_i] \tag{5}$$

where x_R represents the product assumed as arbitrary reference, and n_R is the relative noise for the reference product. In this study, we collected data for 120 months (from 1998 to 2007) for three satellite-based and rain-gauge based products. Then, by calculating the covariance of matrix Y:

$$S = cov(Y) \tag{6}$$

The covariance function calculates the variance for the diagonal elements of matrix Y and covariance for non-diagonal elements. Furthermore, matrix S can be related to the dependent and independent noise matrices that are represented by E (Galindo and Palacio, 2003):

$$S = J.\ E.\ J^T \tag{7}$$

The matrix E is $N \times N$, and matrix J is a $N \times (N-1)$ transformation matrix relating S and R in the described relation. The transformation matrix is given by:

$$J_{(N-1)\times N} = \begin{bmatrix} 1 & 0 & \cdots & 0 & -1 \\ 0 & 1 & & 0 & -1 \\ \vdots & & 1 & & \vdots \\ 0 & 0 & \cdots & 1 & -1 \end{bmatrix}$$

It can be concluded by the structure of the above equation and used matrices that N undetermined parameters in matrix E will remain. As the free-undetermined parameters, we will choose the last column of the noise matrix, which includes $(N-1)$ covariances of the Nth product with other products and the variance of the Nth product (Galindo and Palacio 2003), and the remaining elements can be determined using these free parameters:

$$e_{i,k} = s_{i,k} - e_{N,N} + e_{i,N} + e_{k,N} \qquad i,\ k \in \{1,\ N-1\} \tag{8}$$

The key constraint for restricting the free parameters' solution domain is for matrix E to be positive definite. Tavella and Premoli (1994) proved that this can be possible if and only if the determinant of matrix E is larger than zero:

$$|E| > 0$$

This constraint is the key for only restricting the solution domain; however, we cannot find the free parameters with this constraint only. Using another criterion for solving the given problem is needed in this phase. As Galindo and Palacio (1999) suggested, there are two objective functions. The first one seems to be simple, having the knowledge from the problem:

$$F(\theta) = \sum_{i<k} \frac{e_{i,k}}{|S|^{(N-1)/2}} \qquad \theta \in \{e_{1,N}, e_{2,N},,, e_{N,N}\} \tag{9}$$

The second function has more physical information regarding the problem but it may cause some convexity problems, during the minimization:

$$F(\theta) = \sum_{i<k} \frac{e_{i,k}}{e_{i,i} \bullet e_{k,k}} \qquad \theta \in \{e_{1,N}, e_{2,N},,, e_{N,N}\} \tag{10}$$

Galindo and Palacio (1999) proved that the second objective function does not lead to a unique solution and that it will range in a soft behavior within a small variation. Thus, we choose the first function to solve the problem, which will result in a unique answer but will end up in a unique matrix of E.

In these functions, θ is a set of free parameters that will be calculated after minimization of the objective function. The minimization process is convex because it is following the global minimum of an elliptic paraboloid within the constraint area (Galindo and Palacio, 1999).

Now we can minimize the chosen objective function regarding the defined constraint. The minimization problem can be solved through any method; however, because of the Kuhn-Tucker theorem in handling

inequalities as constraints (Kuhn et al., 1956). The Kuhn-Tucker theorem would be a wise choice for our problem.

The general form of the Kuhn-Tucker theorem is:

$$\text{minimize } f_0(x)$$

$$\text{subject to } f_l(x) \le 0 \qquad (l = 1, 2, \ldots, m) \tag{11}$$

where the function f will take n free parameters (in our case N) and minimize the function regarding m constraints associated with problem (in our case the constraint is $|E| > 0$). Now, by adding m additional variables, i.e., slack variables, to the subject functions, we can convert the inequality form to equality and change the problem to the classical optimization problem

$$\text{minimize } f_0(x)$$

$$\text{subject to } f_l(x) + y_l = 0 \qquad (l = 1, 2, \ldots, m) \tag{12}$$

Let's assume that the $f_p(x)$ for $p = 0, 1, \ldots, m$ are all differentiable. If the function $f_0(x)$ reaches the local minimum subjected to $\{x | f_l(x) \le 0 \;\; (l = 1, \ldots, m)\}$ there should be a Lagrangian multiplier as a vector to satisfy the Kuhn-Tucker conditions stated below:

$$\frac{\partial f_0(x^0)}{\partial x_h} + \sum_{l=1}^{m} \omega_l^0 \frac{\partial f_l(x^0)}{\partial x_h} = 0 \quad (h = 1, 2, \ldots, n) \tag{13}$$

$$f_l(x^0) \le 0 \quad (l = 1, 2, \ldots, m)$$

$$\omega_l^0 f_l(x^0) = 0 \quad (l = 1, 2, \ldots, m)$$

$$u_l^0 \ge 0 \; (l = 1, 2, \ldots, m)$$

x^0 is the point in which the $f_0(x)$ reaches the local minimum and ω^0 is the Lagrangian multiplier vector. The values for the vector are dependent on the subject of the problem. In our case, the subject is $f_l(x) > 0$, which is not the same as the general form of the problem. To solve this, the values of the Lagrangian multiplier should be nonpositive.

Satisfying these conditions will solve the problem of finding the local minimum, which, in our case, is the same as the global minimum.

The SNR is obtained from the noise information retrieved from GTCH, and provides the productivity scale of each product:

$$SNR = \frac{RMS(T)}{RMSE(i)} \tag{14}$$

T represents the time series of each data point from 1998 to 2007. The RMS is Root Mean Square of each product, and RMSE is the uncertainty of each product, which is calculated in the GTCH method.

The benefit of using SNR evaluation is that it will take into account the uncertainty and interrelation of products (Bormann, 2005).

3.2. Extreme indices

Ten precipitation extreme indices introduced by the Expert Team on Climate Change and Detection Indices (ETCCDI; Zhang et al., 2011), are used to show how the PERSIANN-CDR and TRMM-3B42V7 datasets can capture extreme events in the period 1998–2007 (Table 1). The indices are categorized as, Intensity, Absolute Threshold, Wet Spell and Dry Spell.

Similarly, the ten precipitation extreme indices were also calculated for the PERSIANN-CDR, TRMM-3B42V7, and GAUGE datasets for 228 selected pixels (including at least 3 gauges). Then, the annual mean of these parameters was calculated for the ten-year time period for every pixel. In order to compare the dominant behavior of the satellite datasets for detection of precipitation extremes, scatter-plots, correlation coefficients and the RMSE are derived between GAUGE and satellite datasets for the annual means.

3.3. Kolmogorov-Smirnov test

The ECDF for PERSIANN-CDR, TRMM-3B42V7, and GAUGE daily precipitation, as well as dry spells with different thresholds (2.5 mm/day, 5 mm/day, and 10 mm/day) for 7 pixels that include at least 5 gauges (for more accuracy), were calculated. The pixels are chosen based on the differences between the amounts of the SNRs of the datasets located in different geographical locations and different climates of the country (Fig. 1). The Kolmogorov-Smirnov test (K-S test) is a nonparametric test. If the test is used to compare a sample distribution function with a continuous reference-distribution function, it is called a one-sample K-S test, but if the test is used to compare or measure the greatest distance between two samples, it is called a two-sample test. In both cases, the underlying population function is assumed to be continuous. The two-sample test is sensitive to both location and shape of the two-sample CDFs (Corder and Foreman, 2014). In this study, the K-S test is used to determine the greatest distance between the ECDFs of the satellite-product series and the ECDFs of the GAUGE series. The null hypothesis is that the satellite-product ECDFs are from the same distributions as those of the GAUGE distribution.

4. Evaluations and Intercomparison

Although the distributions of the mean-annual precipitation are similar for all datasets, there are some differences (or even contrasts), especially in the higher elevations of the Zagros Mountains and in the low elevations along the coastline of the Caspian Sea (Fig. 2). Specifically, TRMM-3B42V7 and PERSIANN-CDR show the highest amounts of annual precipitation (more than 800 mm and 600 mm, respectively), while CRU shows very low amounts of annual precipitation (in the Zagros Mountains, the precipitation is less than 350 mm and, along the coastline of the Caspian Sea, it is less than 200 mm). These high elevation regions in Zagros Mountains are particularly affected by undercatch of rain (due to wind) and snow by rain-gauges. Similar differences between CRU and Global Historical Climatology Network (GHCN) dataset have been noted before in cold mountainous region in North Asia (Trenberth et al. 2007; Harris, 2014). The wind under-

Table 1
Extreme precipitation indices used in the analysis (as used by Miao et al., 2015).

Category	ID	Definition	Unit
Intensity indices	SDII	Mean daily precipitation from annual wet days	mm/day
	RR90p	The 90th percentile of annual precipitation on wet days (precipitation ≥ 2.5 mm)	mm/day
	Rx1d	Annual maximum 1-day precipitation	mm/day
	Rx5d	Annual maximum 5-day consecutive precipitation	mm/5 days
Absolute threshold indices	R20mm	Annual count of days when precipitation ≥ 20 mm	days
	R10mm	Annual count of days when precipitation ≥ 10 mm	days
	R20mmTOT	Annual total precipitation when precipitation ≥ 20 mm	mm
	R10mmTOT	Annual total precipitation when precipitation ≥ 10 mm	mm
Wet and dry spell indices	CWD	Annual largest number of consecutive days with precipitation ≥ 2.5 mm	days
	CDD	Annual largest number of consecutive days with precipitation < 2.5 mm	days

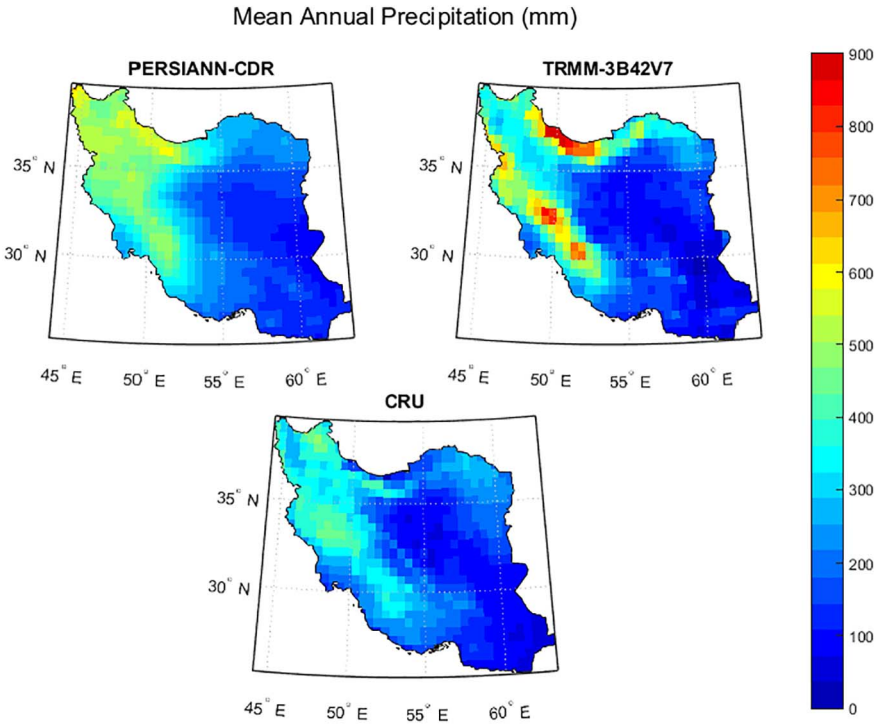

Fig. 2. Mean annual precipitation in millimeter for the period 1998–2007.

catchment along other uncertainties within the gauge measurements justifies the use of GTCH which takes no references as ground-truth. All datasets show similar patterns and approximately the same amounts of precipitation in the arid southeastern and central parts of the country.

The scatter-plots of mean annual precipitation of satellite products versus CRU are shown in Fig. 3. Correlation coefficients and the RMSE are derived between CRU and satellite datasets for the annual means. Although TRMM-3B42V7 and PERSIANN-CDR both overestimate annual precipitation in comparison with CRU data, PERSIANN-CDR is in more agreement with this gauge-based dataset.

4.1. Monthly analysis

In this section, the PERSIANN-CDR, TRMM-3B42V7, and CRU monthly precipitation data over Iran at 0.5°-grid resolution are compared using Monthly MD and Monthly RMSD for the period 1998–2007. Fig. 4 shows the average of monthly precipitation differences for two datasets. The areas for which datasets agree with each other (within 2 mm/month tolerance) are shown in gray. Although CRU and PERSIANN-CDR agree well in the eastern part of the country (with a maximum of up to 5 mm tolerance), PERSIANN-CDR has higher monthly precipitation over CRU in the western and northwestern regions 5–20 (mm/month). In comparison with CRU, TRMM-3B42V7, on the other hand, has lower monthly precipitation over the eastern part of the Zagros Mountains and higher monthly precipitation (30 mm/month) along the coastline of the Caspian Sea, as well as the high elevations in the region west of the Zagros Mountains. In fact, PERSIANN-CDR estimation (with respect to TRMM-3B42V7) has higher amounts in the northwest and central regions and lower amounts along the coastline of the Caspian Sea and high elevations in the west of the Zagros Mountains.

In order to represent dominant spatial patterns of differences in the datasets, the results of RMSD for each pair of datasets are shown in Fig. 5. This figure extracts the areas with the most pronounced differences between datasets. Overall, the high variability between datasets is found along the coastline of the Caspian Sea (mostly the

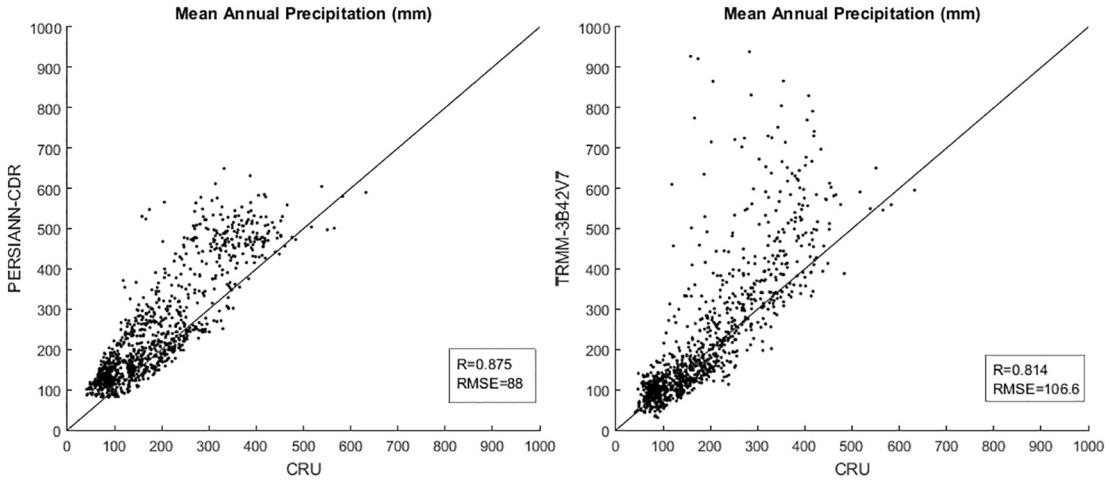

Fig. 3. The scatter-plot of mean annual precipitation of PERSIANN-CDR and TRMM-3B42V7 versus CRU.

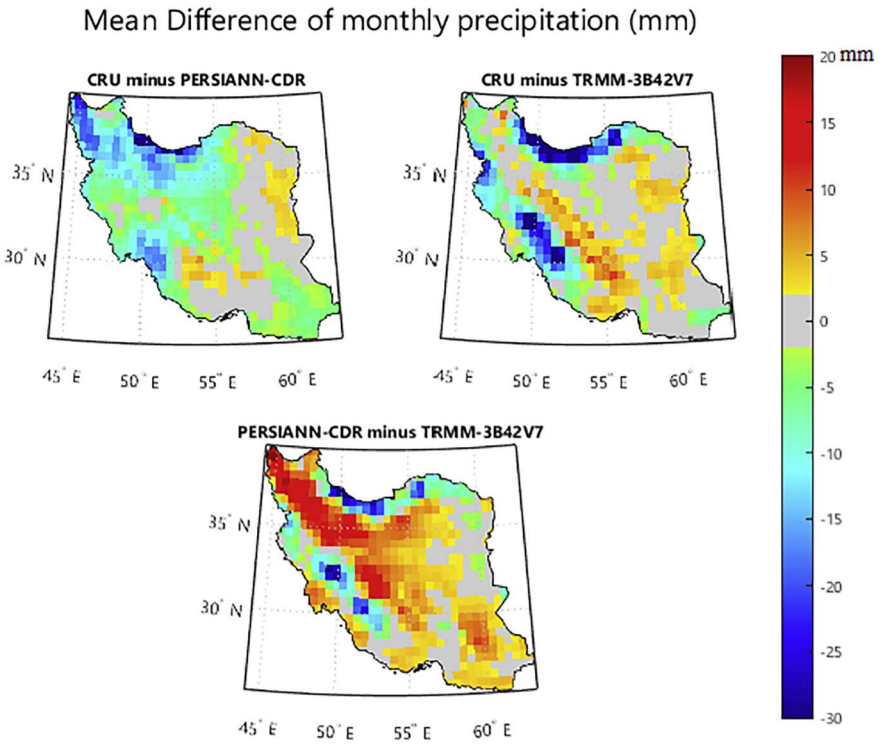

Fig. 4. Mean Difference of monthly precipitations between both pairs of datasets.

western part) and in the high-elevation areas of the Zagros Mountains in the southwest regions which maximum differences between CRU and TRMM-3B42V7 are more than 70 mm/month and between TRMM-3B42V7 and PERSIANN-CDR are equal to 50 mm/month.

In some countries, such as Iran, in which a reliable, long-term in-situ precipitation dataset is inaccessible, the GTCH method could be appropriate for the assessment of satellite products without the need for prior knowledge of the uncertainties. Derived uncertainties (or here noise values) were used with the signals from the same dataset to provide a better signal to noise ratio comparison. Obviously, in wet areas, noise values are higher than in dry areas. To prevent the influence of this phenomenon on the results of the intercomparisons, the SNR of monthly precipitation is calculated at each pixel for all datasets. This parameter is dimensionless, and the dataset with higher SNR values indicates better performances. Fig. 6 shows the results of noise estimate as well as SNR for monthly precipitation of the three datasets.

As shown in Fig. 6, all datasets have high noise in the southwestern region of the country. TRMM-3B42V7 shows a high value of noise in the most parts of the country that is dominant in the west (the Zagros

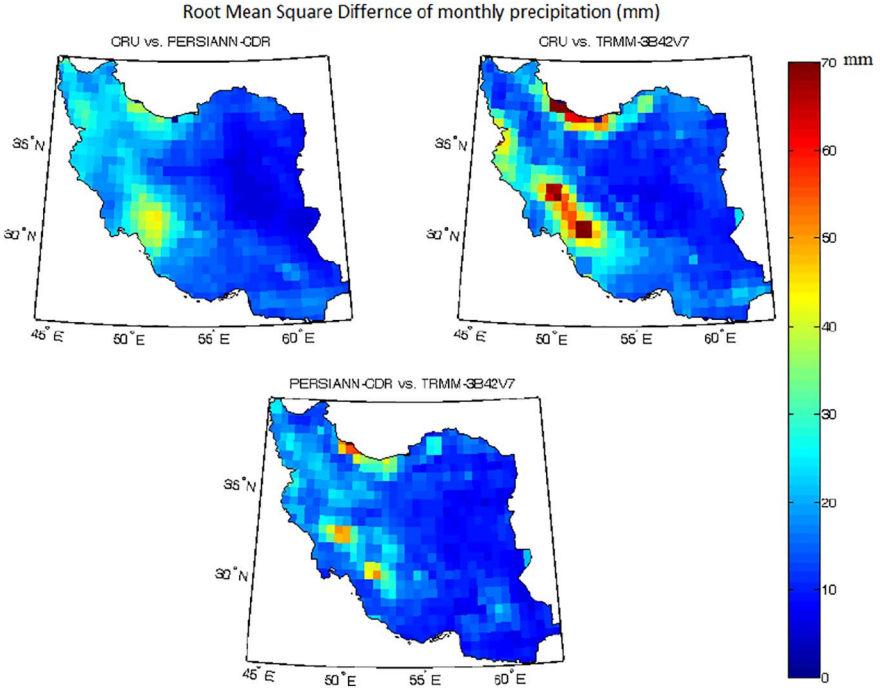

Fig. 5. The RMSD of monthly precipitation between each pair of datasets.

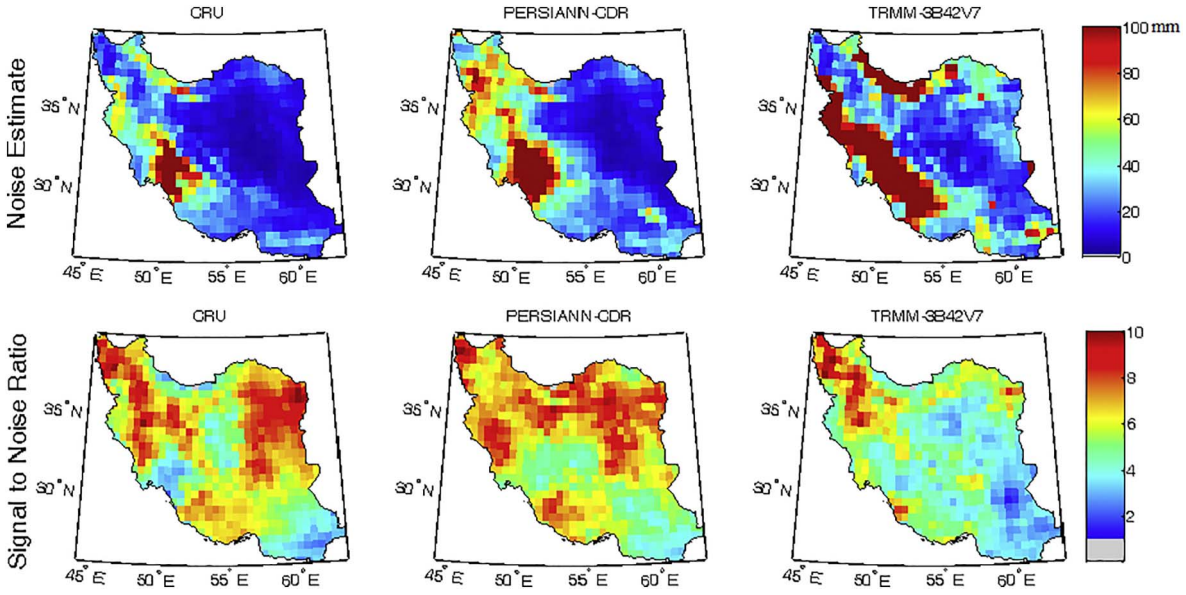

Fig. 6. The noise estimates and SNR values of monthly precipitation using the GTCH method for CRU, PERSIANN-CDR, and TRMM-3B42V7.

Mountains) and north (the coastline of the Caspian Sea). CRU and PERSIANN-CDR show low noise in the central and eastern parts of the country. The analysis of the noise amount is not sufficient to evaluate the datasets because usually, the wet areas show a higher noise magnitude than the dry areas. However, the SNR is more appropriate for evaluating different precipitation products. Based on the GTCH method, PERSIANN-CDR has higher SNR values than TRMM-3B42V7 and CRU, especially in the northern half of Iran. However, TRMM-3B42V7 has better estimation in the northwestern areas, but, in comparison with PERSIANN-CDR, it has poor results in other parts, especially in dry areas in the central and the southeast areas. This result for TRMM-3B42V7 almost agrees with that found in Awange et al. (2015) over Africa, which concluded that, "SNR values are lower in drier areas than the other regions". PERSIANN-CDR shows higher SNR values in dry regions of central Iran than the wet, high-elevation areas in the Zagros Mountains (in the southwest). In fact, the topography and distribution of the dry and wet areas over Iran are different than those in Africa. In comparison with PERSIANN-CDR, CRU has lower SNR especially in the northern (the coastline of the Caspian Sea), central, and the southeastern areas of the country.

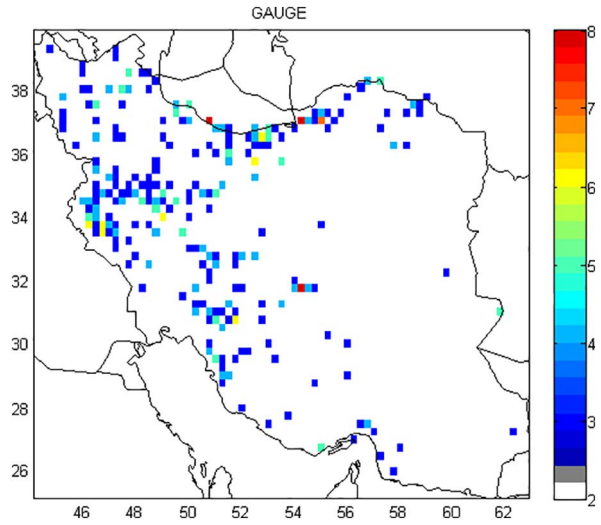

Fig. 7. The location and number of gauges in 228 selected pixels that include at least 3 rain gauges (Katiraie-Boroujerdy et al., 2016).

4.2. Daily analysis

In order to intercompare the extreme precipitation which is important for hydroclimate studies, the annual mean of 10 extreme indices introduced by ETCCDI (Table 1) are calculated for PERSIANN-CDR, TRMM-3B42V7, and GAUGE data for 228 selected pixels that include at least 3 gauges for the period 1998–2007, for which the GAUGE daily dataset is available. The location and the number of gauges which are in each pixel are shown in Fig. 7. As seen in this figure, most of the pixels are located in the more wet western and northern regions of the country, as opposed to the dry eastern areas and the arid central parts of Iran.

Fig. 8 shows the scatter plots for the annual mean of intensity indices for the satellite products and GAUGE data. The correlation (R) and RMSE between satellite products and GAUGE data are shown in the boxes. However, TRMM-3B42V7 overestimates most of the intensity indices; PERSIANN-CDR underestimates these extremes. The spatial correlation between the PERSIANN-CDR and GAUGE annual mean of the intensity indices are between 0.6349 (for SDII) to 0.7791 (for Rx1d) and the RMSEs vary from 3.59 mm/day for SDII to 30.56 mm/5 day for Rx5d. The statistical results for TRMM-3B42V7 are similar (R = 0.7661–0.8311 and RMSE = 3.29 mm/day-21.23 mm/5 day). On the other hand, the statistical results for the annual mean of absolute indices (shown in Fig. 9) indicate that TRMM-3B42V7 can capture these extremes better than PERSIANN-CDR. Again, PERSIANN-CDR underestimates these extremes, especially in wet regions. As shown in Fig. 10, the scatter-plots and statistical results indicate that PERSIANN-CDR and TRMM-3B42V7 have similar correlation coefficients and the RMSEs in capturing consecutive dry and wet spell indices. In fact, both satellite products show better results for the annual mean of consecutive dry spells than wet spells.

For the purpose of intercomparison of daily-distribution functions, the ECDF of daily precipitation and dry spells with different thresholds (2.5, 5, 10 mm/day) in some pixels (shown in Fig. 1) are calculated. The selected pixels include at least 5 gauges (for more accuracy) for PERSIANN-CDR, TRMM-3B42V7, and GAUGE observations. The locations of the pixels are selected based on the monthly results (SNR and MD) of PERSIANN-CDR and TRMM-3B42V7 in different parts of the country (Figs. 6 and 5).

As mentioned before, the largest differences between PERSIANN-CDR and TRMM-3B42V7 and their SNR are considered along the

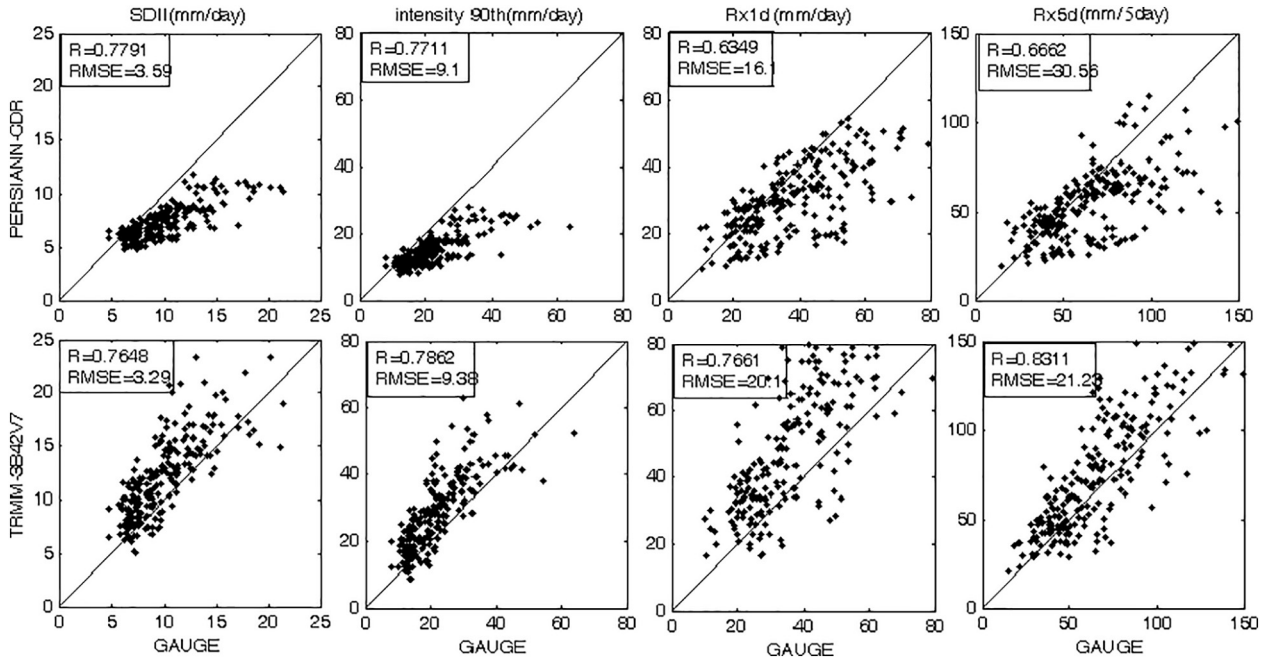

Fig. 8. The scatter-plots between PERSIANN-CDR, TRMM-3B42V7, and GAUGE for annual mean of intensity indices provided in Table 1 for the period 1998–2007. The R and RMSE represent are correlation and root mean square error of the satellite products (based on GAUGE), respectively.

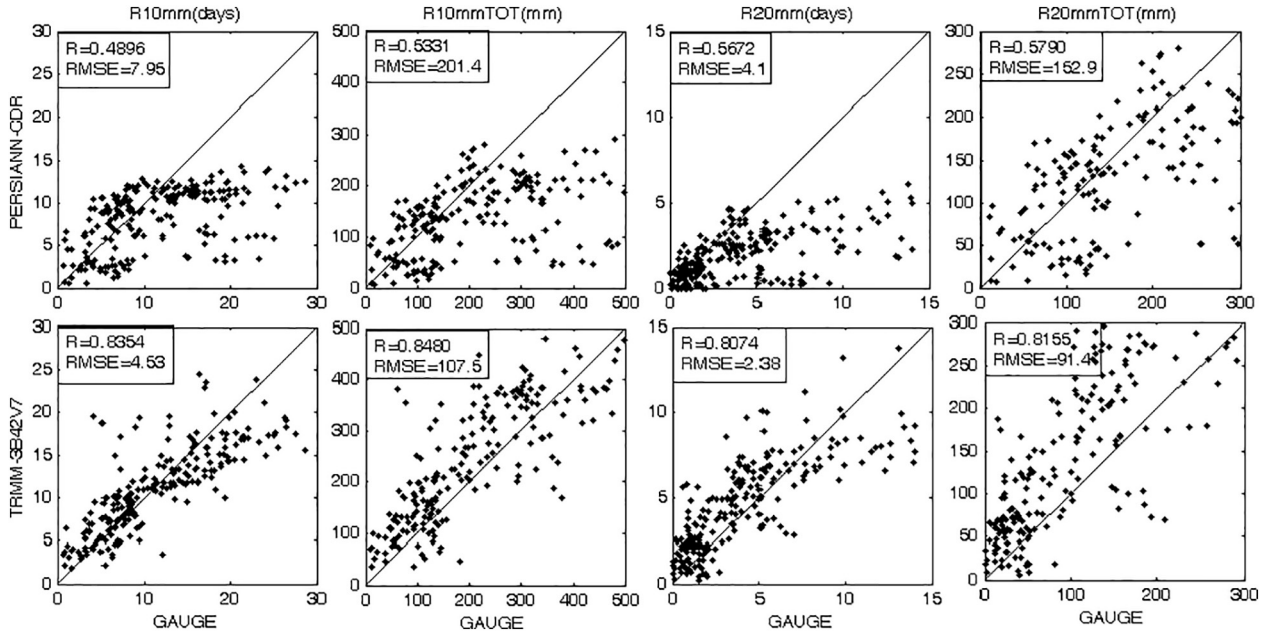

Fig. 9. Same as Fig. 8, but for annual mean of absolute extremes provided in Table 1.

coastline of the Caspian Sea (N), west and east of the Zagros Mountains (W1 and W2, respectively), the northwest (NW), the northeast (NE), and the high-elevation areas of the Zagros Mountains in the south-western (SW) region of the country. Fig. 6 shows higher SNR for PERSIANN-CDR than TRMM-3B42V7 in dry and arid parts in the eastern and the central areas, but there is a large gap of gauge data in these regions. The only available pixel with 5 gauges to represent the dry regions (See box E in fig. 3) was included in the verification study. However, it should be pointed out that this pixel showed different pattern from the rest of verification dataset due to its extreme dryness. Another pixel (see box S in fig. 3) along the coastline of the Persian Gulf was also selected to represent the southern region of the country. We note that both satellite datasets show similar SNR along this region. As mentioned in Section 3.2, the Kolmogorov-Smirnov test is used to determine the similarity of GAUGE and satellite-product ECDFs (95% significance).

Fig. 11 shows the results of ECDFs of daily precipitation with 3 different thresholds for GAUGE, TRMM-3B42V7, and PERSIANN-CDR data for 8 selected pixels. The significant similarities of ECDFs of the satellite data to the GAUGE data (based on the Kolmogorov-Smirnov test) are shown in the text box in each diagram. The results show that PERSIANN-CDR mostly underestimates and TRMM-3B42V7 overestimates daily precipitation. The ECDF distances reduce when the daily-rainfall threshold increases or, in other words, the ECDFs for heavier daily rainfalls match more than lighter daily rainfall.

Although the regional performances of the satellite products on monthly scales (SNR) agree with the daily evaluations in most pixels, there are some disagreements in a few pixels. For example, the satellite

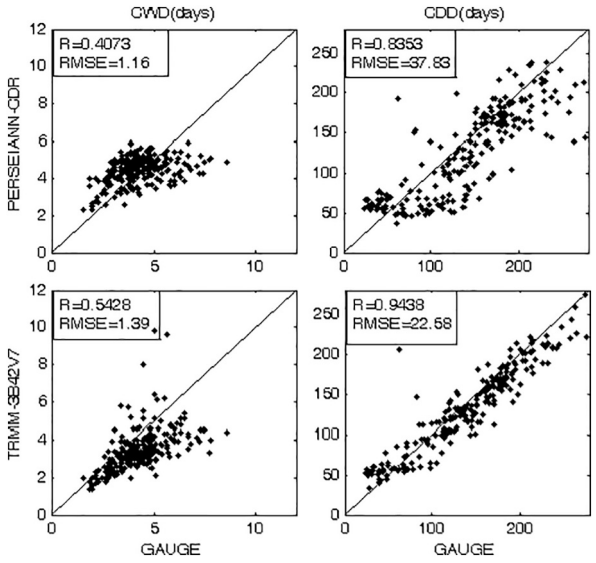

Fig. 10. Same as Fig. 8 but for annual mean of consecutive dry and wet spell extremes provided in Table 1.

products have similar SNR in pixel S (along the coastline of the Persian Gulf) but, in the daily scale, TRMM-3B42V7 has better results. Furthermore, TRMM-3B42V7 has small SNR in pixel E, but Fig. 11 shows that the ECDF is significantly close to GAUGE data for heavy precipitation. On the other hand, PERSIANN-CDR has high SNR in pixel N (along the coastline of the Caspian Sea), and its ECDF is closer to GAUGE than the ECDF of TRMM-3B42V7. As Fig. 11 shows, the ECDFs of PERSIANN-CDR on both sides of the Zagros Mountains (W1, W2) are very close to those of the GAUGE data, even though the results are significant only for heavy rainfall. In NW and NE, PERSIANN-CDR results are relatively reliable.

Referring to Figs. 4 and 5 the most differences between monthly precipitation of PERSIANN-CDR and TRMM-3B42V7 are in the high-elevation areas of the Zagros Mountains (SW) and the low-elevation of the northern (less than sea-surface level) areas (N) that are wet (more than 700 mm annual precipitation). The comparisons of the ECDFs of daily precipitation of satellite products and GAUGE data in SW and N show that despite the fact that PERSIANN-CDR underestimates daily rainfall in both areas, it still has better results than TRMM-3B42V7 in N.

Fig. 12 shows the results of ECDFs of dry spells with 3 different daily-precipitation thresholds for the GAUGE, TRMM-3B42V7, and PERSIANN-CDR data for 8 selected pixels. The satellite products underestimate the duration of dry spells in the dry areas (S and E), but the results improve when the daily-rainfall thresholds increase. On the other hand, satellite products (especially PERSIANN-CDR) overestimate the duration of dry spells in wet areas (SW, N, and NE), and the results become worse when the daily-rainfall thresholds increase. The greatest differences between ECFDs are in NE and NW for dry spells with a 10 mm/day threshold that, respectively, PERSIANN-CDR and TRMM-3B42V7 overestimate these dry spells dominantly, while the other one is close to GAUGE data.

5. Summary and conclusions

In this study, the GTCH method is used to compare the two satellite-based precipitation datasets (PERSIANN-CDR and TRMM-3B42V7) and a gauge-based precipitation dataset (CRU) in monthly scales. Although this method does not need a reference dataset, it requires at least 3 data series. Obviously, GTCH might be functional for mountainous and desert areas, such as those found in Iran, where continuous reliable in situ data are not available. The selection of the study period was dictated by the period for which gauge data was available (1998 to 2007). The mean difference, the root mean square difference, and the SNR of monthly precipitation for each dataset in each pixel are calculated (based on the GTCH method). For daily assessment in the first stage, we only considered the daily-rainfall data of the GAUGE data-set (as reference) for 228 pixels (0.25°) that include at least 3 gauges. The annual mean of 10 extreme indices introduced by ETCCDI (Table 1) was calculated for PERSIANN-CDR, TRMM-3B42V7, and GAUGE data in these pixels. In order to understand how these satellite products agree with GAUGE data in daily-rainfall distribution, we calculated the ECDF of daily precipitation and the dry spells with different thresholds (2.5, 5, 10 mm/day) in some pixels that include at least 5 gauges (for more accuracy) for PERSIANN-CDR and TRMM-3B42V7.

The results show that in comparison to CRU, TRMM-3B42V7 and PERSIANN-CDR both overestimate monthly precipitation over the northern region and the high elevation southwest regions of the country by more than 30 mm/month and 5 mm/month respectively. It must be mentioned that as a consequence of complicated topography in both areas estimation of the areal precipitation is difficult. On the other hand in the same regions, PERSIANN-CDR underestimates precipitation as compared to TRMM-3B42V7 by about 25 mm/month but it overestimates by about 20 mm/month in the eastern parts of the Zagros Mountain.

The RMSD of monthly precipitation between each pair of datasets shows that the largest differences (between 30 mm/month to more than 70 mm/month) are along the coastline of the Caspian Sea (mostly the western part) and the high-elevation areas of the Zagros Mountains in the southwest region of Iran. Respectively, PERSIANN-CDR and TRMM-3B42V7 use GPCP and Global Precipitation Climatology Centre (GPCC) monthly data for adjustment purposes. The high value of MD and RMSD between these satellite products indicates the differences between GPCP and GPCC monthly data over these areas. The differences between GPCP and GPCC are not unique to our study area and have been reported by Prein and Gobiet (2017) over some parts of Europe. The results of monthly evaluations based on GTCH show that PERSIANN-CDR has higher SNR than TRMM-3B42V7 and CRU, especially in the northern half of the country. TRMM-3B42V7 has lower SNR in comparison with other dataset, especially in the east, southeast, and central regions. The scatter-plots and statistical analyses (R and RMSE) of mean annual daily-extreme indices show that TRMM-3B42V7 and PERSIANN-CDR have similar results for intensity indices and consecutive wet and dry spells, but TRMM-3B42V7 can capture the annual mean of the absolute indices (number of wet days that daily precipitation > 10 mm, 20 mm) better than PERSIANN-CDR. In fact, PERSIANN-CDR uses GPCP 2.5° monthly data for adjustment which are coarser than GPCC 1° monthly data that TRMM-2B42V7 uses. Perhaps this might be one of the reasons that PERSIANN-CDR doesn't capture extremes as well as TRMM-3B42V7. The results for daily-rainfall distribution functions show that the ECDFs for heavier daily rainfalls of satellite products are more closely matched to the GAUGE data than the ECDFs of the lighter daily rainfall. As Fig. 11 shows, in most selected pixels, the ECDFs of the daily rainfall of PERSIANN-CDR are closer to the ECDFs of daily rainfall of GAUGE (only some ECDFs are significant) than the ECDFs of the daily rainfall of TRMM-3B42V7. The results for dry spells show that, in most pixels, the ECDFs of satellite products are similar to GAUGE and become closer as the daily-precipitation threshold increases (except only in the southwestern, northern and northeastern areas for PERSIANN-CDR). This means that the satellite products (especially PERSIANN-CDR) overestimate the duration of dry spells in wet areas (SW, N, and NE), and the results become worse when the daily-rainfall threshold increases.

In summary, the main conclusions that may be inferred from this analysis are:

- PERSIANN-CDR has higher SNR than TRMM-3B42V7 and CRU in the monthly scale, especially in the northern half of Iran.

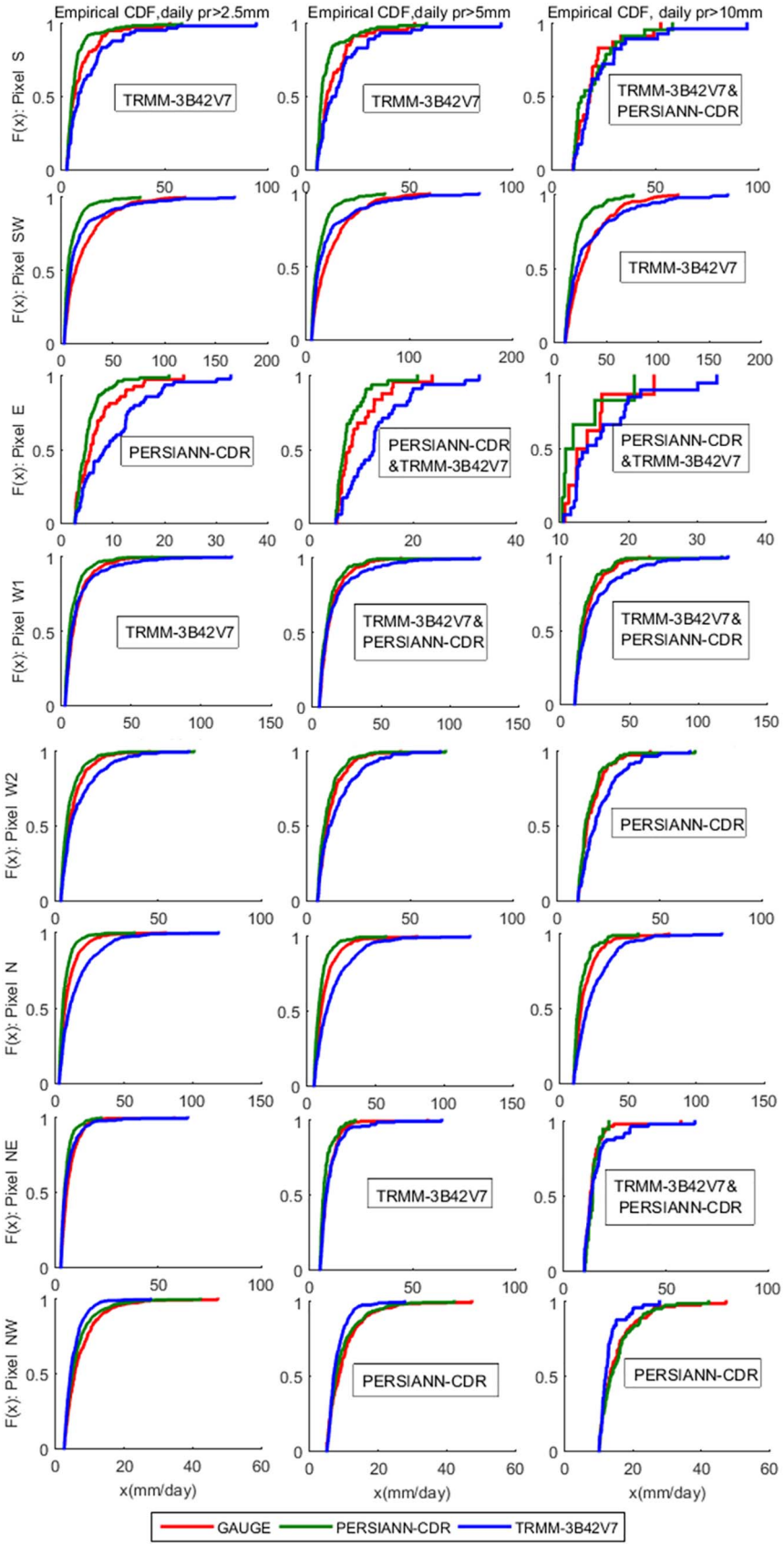

Fig. 11. The comparisons of the ECDFs of daily precipitation (with different thresholds: 2.5, 5, 10 mm/day) of PERSIANN-CDR, TRMM-3B42V7, and GAUGE data. The significant (95%) similar satellite products series based on the Kolmogorov-Smirnov test are shown in text boxes.

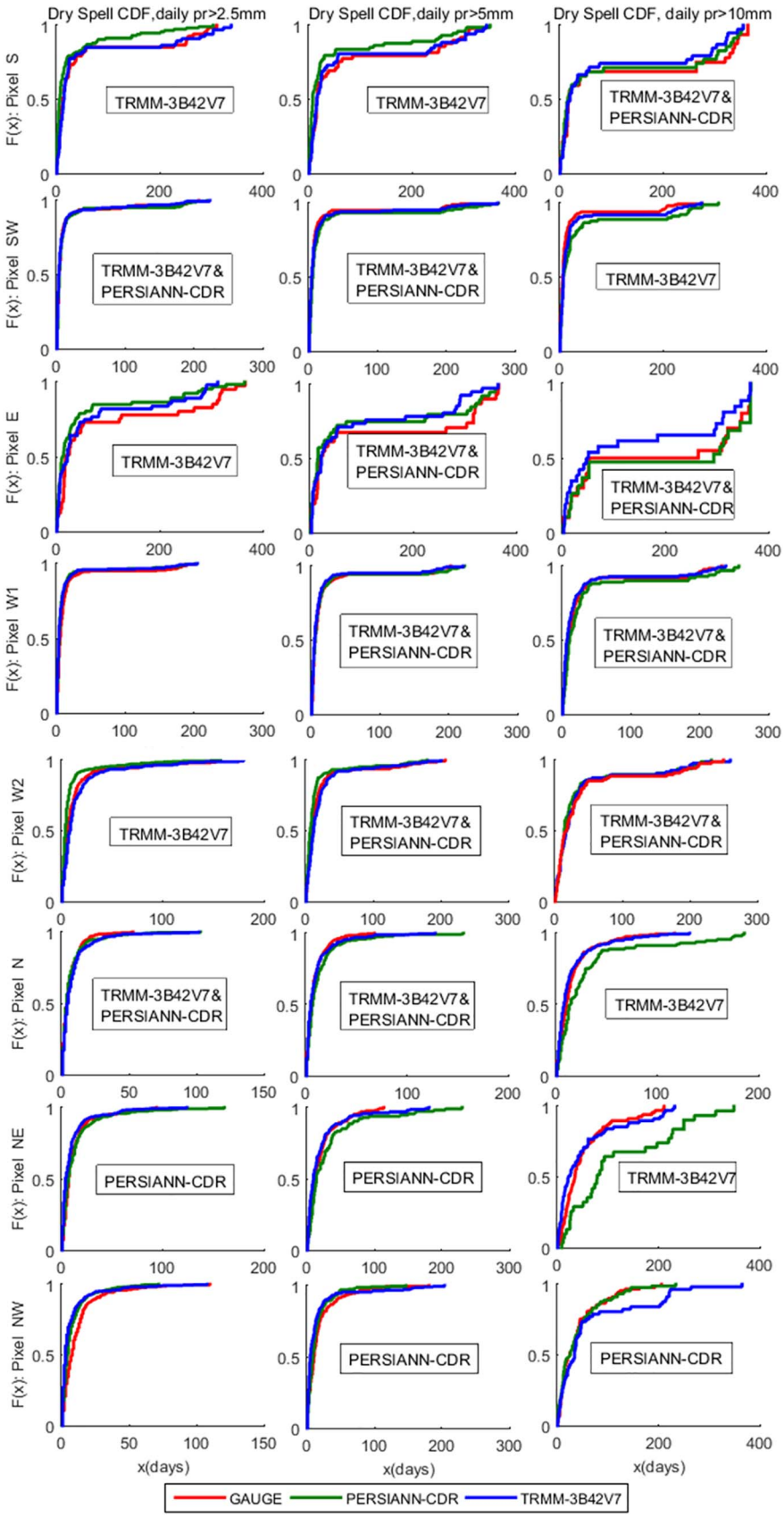

Fig. 12. The comparisons of the ECDFs of dry spells (with different daily-precipitation thresholds: 2.5, 5, 10 mm/day) of PERSIANN-CDR, TRMM-3B42V7, and GAUGE data. The significant (95%) similar satellite-product series based on the Kolmogorov-Smirnov test are shown in text boxes.

- TRMM-3B42V7 captures extreme indices better than PERSIANN-CDR, except some intensity indices, for which PERSIANN-CDR has better results.
- The ECDFs for dry spells of PERSIANN-CDR are similar to those of GAUGE and become closer as the daily-precipitation threshold increases (except for the north and north eastern parts of the country).
- In addition, more research needs to be conducted to improve and assess the application of this method in precipitation datasets.

The primary purpose of this investigation was to evaluate the efficacy of the 33 + years of PERSIANN-CDR for potential applications for climate studies and extreme hydrologic analysis, such as flood frequency etc. The evaluations against TRMM and GAUGE datasets, which were available for nearly 10 years of overlap, showed that, indeed, PERSIANN-CDR is a valuable, high-resolution climate data record and can be employed for various applications, especially for most areas with scarce in-situ observations.

References

Adler, R.F., Huffman, G.J., Chang, A., Ferraro, R., Xie, P., Janowiak, J., Rudolf, B., Schneider, U., Curtis, S., Bolvin, D., Gruber, A., Susskind, J., Arkin, P., 2003. The version 2 global precipitation climatology project (GPCP) monthly precipitation analysis (1979–present). J. Hydrometeorol. 4, 1147–1167.

Adler, R.F., Kidd, C., Petty, G., Morissey, M., Goodman, H.M., 2001. Intercomparison of global precipitation products: the third precipitation intercomparison project (PIP-3). Bull. Am. Meteorol. Soc. 82, 1377–1396.

Arkin, P.A., Xie, P., 1994. The global precipitation climatology project: first algorithm intercomparison project. Bull. Am. Meteorol. Soc. 75, 401–419.

Ashouri, H., Hsu, K.L., Sorooshian, S., Braithwaite, D.K., Knapp, K.R., Cecil, L.D., Nelson, B.R., Prat, O.P., 2015. PERSIANN-CDR: daily precipitation climate data record from multi-satellite observations for hydrological and climate studies. Bull. Am. Meteorol. Soc. 96, 69–83. http://dx.doi.org/10.1175/BAMS-D-13-00068.1.

Awange, J.L., Ferreira, V.G., Forootan, E., Khandu, Andam-Akorful S.A., Agutu, N.O., He, X.F., 2015. Uncertainties in remotely sensed precipitation data over Africa. Int. J. Climatol. 36, 303–323. http://dx.doi.org/10.1002/joc.4346.

Bormann, H., 2005. Evaluation of hydrological models for scenario analyses: signal-to-noise-ratio between scenario effects and model uncertainty. Adv. Geosci. 5, 43–48.

Ciach, G.J., Krajewski, W.F., 2006. Analysis and modeling of spatial correlation structure of small-scale rainfall in central Oklahoma. Adv. Water Resour. 29, 1450–1463. http://dx.doi.org/10.1016/j.advwatres.2005.11.003.

Conti, L.F., Hsu, K.L., Noto, L.V., Sorooshian, S., 2014. Evaluation and comparison of satellite precipitation estimates with reference to a local area in the Mediterranean Sea. Atmos. Res. 138, 189–204. http://dx.doi.org/10.1016/j.atmosres.2013.11.011.

Corder, G.W., Foreman, D.I., 2014. Nonparametric Statistics: a Step-by-Step Approach, Wiley. 978-1118840313.

Galindo, F.J., Palacio, J., 1999. Estimating the instabilities of N correlated clocks; In: Proceedings of the 31st Annual Precise Time and Time Interval (PTTI) Meeting. Real Instituto y Observatorio de la Armada, Dana point, CA, pp. 285–296.

Galindo, F.J., Palacio, J., 2003. Post-processing ROA data clocks for optimal stability in the ensemble timescale. Metrologia 40 (3), S237–S244. http://dx.doi.org/10.1088/0026-1394/40/3/301.

Grubbs, F.E., 1948. On estimating precision of measuring instruments and product variability. J. Am. Stat. Assoc. 43 (242), 243–264.

Gruber, A., Su, C.H., Zwieback, S., Crow, W., Dorigo, W., Wagner, W., 2016. Recent advances in (soil moisture) triple collocation analysis. Int. J. Appl. Earth Obs. Geoinf. 45, 200–211. http://dx.doi.org/10.1016/j.jag.2015.09.002.

Habib, E., Krajewski, W.F., 2002. Uncertainty analysis of the TRMM ground validation radar-rainfall products: application to the TEFLUN-B field campaign. J. Appl. Meteorol. 41, 558–572.

Habib, E., Krajewski, W.F., Kruger, A., 2001. Sampling errors of tipping bucket rain gauge measurements. J. Hydrol. Eng. 6 (2), 159–166.

Harris, I., Jones, P.D., Osborn, T.J., Lister, D.H., 2014. Updated high-resolution grids of monthly climatic observations - the CRU TS3.10 dataset. Int. J. Climatol. 34, 623–642. http://dx.doi.org/10.1002/joc.3711.

Hossain, F., Huffman, G.J., 2008. Investigating error metrics for satellite rainfall data at hydrologically relevant scales. J. Hydrometeorol. 9, 563–575.

Huffman, G.J., Adler, R.F., Bolvin, D.T., Gu, G., Nelkin, E.J., Bowman, K.P., Hong, Y., Stocker, E.F., Wolff, D.B., 2007. The TRMM Multisatellite precipitation analysis (TMPA): quasi-global, multiyear, combinedsensor precipitation estimates at fine scales. J. Hydrometeorol. 8 (1), 38–55.

Huffman, G.J., Adler, R.F., Morrissey, M., Bolvin, D.T., Curtis, S., Joyce, R., McGavock, B., Susskind, J., 2001. Global precipitation at one-degree daily resolution from multi-satellite observations. J. Hydrometeorol. 2 (1), 36–50.

Javanmard, S., Yatagai, A., Nodzu, M.I., BodaghJamali, J., Kawamoto, H., 2010. Comparing high-resolution gridded precipitation data with satellite rainfall estimates of TRMM 3B42 over Iran. Adv. Geosci. 25, 119–125. http://dx.doi.org/10.5194/adgeo-25-119-2010.

Katiraie-Boroujerdy, P.S., Ashouri, H., Hsu, K.L., Sorooshian, S., 2016. Trends of precipitation-extreme indices over a subtropical semi-arid area using PERSIANN-CDR. Theor. Appl. Climatol. http://dx.doi.org/10.1007/s00704-016-1884-9.

Katiraie-Boroujerdy, P.S., Nasrollahi, N., Hsu, K.L., Sorooshian, S., 2013. Evaluation of satellite-based precipitation estimation over Iran. J. Arid Environ. 97, 205–219. http://dx.doi.org/10.1016/j.jaridenv.2013.05.013.

Kidd, C., Bauer, P., Turk, J., Huffman, G.J., Joyce, R., Hsu, K.L., Braithwaite, D., 2012. Intercomparison of high-resolution precipitation products over Northwest Europe. J. Hydrometeorol. 13, 67–83. http://dx.doi.org/10.1175/JHM-D-11-042.1.

Koot, L., Viron, O.D., Dehant, V., 2006. Atmospheric angular momentum time-series: characterization of their internal noise and creation of a combined series. J. Geod. 79 (12), 663–674. http://dx.doi.org/10.1007/s00190-005-0019-3.

Krajewski, W.F., et al., 2006. DEVEX-disdrometer evaluation experiment: basic results and implications for hydrologic studies. Adv. Water Resour. 29, 311–325. http://dx.doi.org/10.1016/j.advwatres.2005.03.018.

Kuhn, H.W., Tucker, A.W., Dantzig, G.B., 1956. Linear inequalities and related systems. 38 Princeton university press.

Larocca, R., 2010. Gauss-Markov theorem. In: Salkind, N. (Ed.), Encyclopedia of Research Design. SAGE Publications, Inc., Thousand Oaks, CA, pp. 529–534. http://dx.doi.org/10.4135/9781412961288.n164.

Liu, X., Yang, T., Hsu, K., Liu, C., Sorooshian, S., 2016. Evaluating the streamflow simulation capability of PERSIANN-CDR daily rainfall products in two river basins on the Tibetan plateau. Hydrol. Earth Syst. Sci. Discuss. http://dx.doi.org/10.5194/hess-2016-282.

Miao, C., Ashouri, H., Hsu, K.L., Sorooshian, S., Duan, Q., 2015. Evaluation of the PERSIANN-CDR rainfall estimates in capturing the behavior of extreme precipitation events over China. J. Hydrometeorol. 16 (1). http://dx.doi.org/10.1175/JHM-D-14-0174.1.

Moazami, S., Golian, S., Kavianpour, M.R., Hong, Y., 2013. Comparison of PERSIANN and V7 TRMM multi-satellite precipitation analysis (TMPA) products with rain gauge data over Iran. Int. J. Remote Sens. 34, 8156–8171. http://dx.doi.org/10.1080/01431161.2013.833360.

New, M., Hulme, M., Jones, P., 1999. Representing twentieth century space–time climate variability. Part I: development of a 1961–90 mean monthly terrestrial climatology. J. Climate 12, 829–856.

Prein, A.F., Gobiet, A., 2017. Impacts of uncertainties in European gridded precipitation observations on regional climate analysis. Int. J. Climatol. 37, 305–327. http://dx.doi.org/10.1002/joc.4706.

Prakash, S., Mitra, A.K., AghaKouchak, A., Pai, D.S., 2015. Error characterization of TRMM Multisatellite precipitation analysis (TMPA-3B42) products over India for different seasons. J. Hydrol. 529 (3), 1302–1312. http://dx.doi.org/10.1016/j.jhydrol.2015.08.062.

Premoli, A., Tavella, P., 1993. A revisited 3-cornered hat method for estimating frequency standard instability. IEEE Trans. Instrum. Meas. 42, 7–13.

Shen, Y., Xiong, A.Y., Wang, Y., Xie, P.P., 2010. Performance of high-resolution satellite precipitation products over China. J. Geophys. Res.-Atmos. 115, D02114. http://dx.doi.org/10.1029/2009JD012097.

Sorooshian, S., Hsu, K.L., Gao, X., Gupta, H.V., Imam, B., Braithwaite, D., 2000. Evaluation of PERSIANN system satellite-based estimates of tropical rainfall. Bull. Am. Meteorol. Soc. 81, 2035–2046. http://dx.doi.org/10.1175/1520-0477(2000)081<2035:EOPSSE>2.3.CO;2.

Tapiador, F.J., Turk, F.J., Petersen, W., Hou, A.Y., García-Ortega, E., Machado, L.A.T., Angelis, C.F., Salio, P., Kidd, C., Huffman, G.J., de Castro, M., 2012. Global precipitation measurement: methods, datasets and applications. Atmos. Res. 104, 70–97.

Tavella, P., Premoli, A., 1994. Estimating the instabilities of N clocks by measuring differences of their readings. Metrologia 30 (5), 479. http://dx.doi.org/10.1088/0026-1394/30/5/003.

Tian, Y., Peters-Lidard, C.D., Eylander, J.B., Joyce, R.J., Huffman, G.J., Adler, R.F., Hsu, K.L., Turk, F.J., Garcia, M., Zeng, J., 2009. Component analysis of errors in satellite-based precipitation estimates. J. Geophys. Res. 114, D24101. http://dx.doi.org/10.1029/2009JD011949.

Tong, K., Su, F., Yang, D., Zhang, L., Hao, Z., 2014. Tibetan plateau precipitation as depicted by gauge observations, reanalyses and satellite retrievals. Int. J. Climatol. 34, 265–285. http://dx.doi.org/10.1002/joc.3682.

Trenberth, K.E., Jones, P.D., Ambenje, P., Bojariu, R., Easterling, D., Klein Tank, A., Parker, D., Rahimzadeh, F., Renwick, J.A., Rusticucci, M., Soden, B., Zhai, P., 2007. Observations: surface and atmospheric climate change. In: Solomon, S., Qin, D., Manning, M., Chen, Z., Marquis, M., Averyt, K.B., Tignor, M., Miller, H.L. (Eds.), Climate Change 2007: the Physical Science Basis. Contribution of Working Group I to the Fourth Assessment Report of the Intergovernmental Panel on Climate Change. Cambridge University Press, Cambridge, United Kingdom and New York, NY, USA.

Villarini, G., Mandapaka, P.V., Krajewski, W.F., Moore, R.J., 2008. Rainfall and sampling errors: a rain gauge perspective. J. Geophys. Res. 113, D11102. http://dx.doi.org/10.1029/2007JD009214.

Wood, S.J., Jones, D.A., Moore, R.J., 2000. Accuracy of rainfall measurement for scales of hydrological interest. Hydrol. Earth Syst. Sci. 4, 531–543. http://dx.doi.org/10.5194/hess-4-531-2000.

Xue, X., Hong, Y., Limaye, A., Gourley, J., Huffman, G., Khan, S., Dorji, C., Chen, S., 2013. Statistical and hydrological evaluation of TRMM-based multi-satellite precipitation analysis over the Wangchu Basin of Bhutan: are the latest satellite precipitation products 3B42V7 ready for use in ungauged basins? J. Hydrol. 499, 91–99.

Yong, B., Ren, L.L., Hong, Y., Gourley, J.J., Tian, Y.D., Huffma, G.J., Chen, X., Wang, W.G., Wen, Y.X., 2013. First evaluation of the climatological calibration algorithm in the real-time TMPA1-RT precipitation estimates over two basins at high and low latitudes. Water Resour. Res. 49, 2461–2472. http://dx.doi.org/10.1002/wrcr.

20246.
Zhang, X., Alexander, L., Hegerl, G.C., Jones, P., Tank, A.K., Peterson, T.C., Trewin, B., Zwiers, F.W., 2011. Indices for monitoring changes in extremes based on daily temperature and precipitation data. Wiley Interdiscip. Rev. Clim. Chang. 2 (6), 851–870. http://dx.doi.org/10.1002/wcc.147.
Zhu, Q., Xuan, W., Liu, L., Xu, Y.-P., 2016. Evaluation and hydrological application of precipitation estimates derived from PERSIANN-CDR, TRMM 3B42V7, and NCEP-CFSR over humid regions in China. Hydrol. Process. http://dx.doi.org/10.1002/hyp.10846.